Enhanced PFM-PSM Hybrid Control of CLLC Resonant Converter for Electric Vehicles: Comprehensive Study and Verification

Issac Kim, *Member, IEEE*, Won-Yong Jang, *Student Member, IEEE*, Seung-Jun Lee, *Student Member, IEEE*, and Jung-Wook Park, *Senior Member, IEEE*

***Abstract*—The conventional *CLLC* resonant converters have been generally operated by the pulse-frequency modulation (PFM) method, which changes switching frequency according to the load conditions. However, it causes high switching losses and the first harmonic approximation error, particularly for step-down operations. To handle these issues, several studies, which combines the PFM and phase-shift modulation (PSM) methods, have been reported. Nevertheless, they still have the problem with so-called *inoperative region*, which degrades overall efficiency and reliability during mode changes in wide ranges of voltage. To overcome this limitation, this article proposes the new voltage conversion ratio (VCR) based PFM-PSM hybrid control (VFSHC) method for the *CLLC* resonant converters applied to electric vehicles. It can effectively eliminate the *inoperative region* by changing the PFM and PSM methods based on the reference VCR, which is mathematically determined. Therefore, two methods can be changed seamlessly and successfully without causing undesired transients. Also, it is able to improve overall efficiency by applying the PSM method when the required VCR is lower than the reference VCR. The comprehensive study of proposed VFSHC method is theoretically made, and its practical effectiveness is verified by experimental tests on the hardware prototype of 1.5 KW.**

***Index Terms*—*CLLC* resonant converter, electric vehicle (EV), hybrid control method, phase-shift modulation (PSM), pulse-frequency modulation (PFM), voltage conversion ratio (VCR), wide voltage range.**

NOMENCLATURE

M	Required VCR.
M_{ref}	Reference VCR.
$M_{\max}$	Maximum VCR.
$M_{\min}$	Minimum VCR.
M_{fr_PFM}	VCR at resonant frequency with PFM method.
$M_{\max\_\mathrm{PSM}}$	Maximum VCR with PSM method.
f_s	Operating switching frequency.
$f_{s,\min}$	Minimum switching frequency.
$f_{s,\max}$	Maximum switching frequency.
f_r	Resonant frequency.
f_{tr}	Transition frequency.
P_{sw_loss}	Switching loss.
$P_{sw,\max\cdot\mathrm{PFM}}$	Maximum switching loss with PFM method.
$P_{sw,\min}$	Minimum switching loss
$P_{sw,\max\cdot\mathrm{VFSHC}}$	Maximum switching loss with proposed VFSHC method.
V_o	Output voltage.
$V_{o,\max}$	Maximum output voltage.
$V_{o,\max\_\mathrm{PSM}}$	Maximum output voltage with PSM method.
V_{o,fr_PFM}	Output voltage at resonant frequency with PFM method.
$V_{o,\min}$	Minimum output voltage.
V_{ref}	Reference voltage.
V_H	Required voltage of HVB.
D	Duty ratio.
$D_{\max}$	Maximum duty ratio.
$D_{\min}$	Minimum duty ratio.
V_{gs}	Gate-source voltage.

Manuscript received 18 March 2024; revised 26 May 2024; accepted 14 July 2024. Date of publication 17 July 2024; date of current version 4 September 2024. This work was supported by the National Research Foundation, Ministry of Science and ICT, South Korea, under Grant 2020R1A3B2079407 and Grant RS-2023-00218377. Recommended for publication by Associate Editor S. S. Williamson. This paper was presented in part at the IEEE Energy Conversion Congress and Exposition, Nashville, TN, USA, October 29–November 2, 2023 [DOI: 10.1109/ECCE53617.2023.10362259]. *(Issac Kim and Won-Yong Jang are co-first authors.) (Corresponding author: Jung-Wook Park.)*

The authors are with the Department of Electrical and Electronics Engineering, Yonsei University, Seoul 120-749, South Korea (e-mail: dufgufska2@yonsei.ac.kr; bindung1@yonsei.ac.kr; dltmdwns0199@yonsei.ac.kr; jungpark@yonsei.ac.kr).

Color versions of one or more figures in this article are available at https://doi.org/10.1109/TPEL.2024.3429530.

Digital Object Identifier 10.1109/TPEL.2024.3429530

I. INTRODUCTION

THE electric vehicles (EVs) have attracted significant attentions over last two decades due to the global issues on carbon neutrality. As a result, many researches on the on-board charger (OBC) applied to the EVs have been conducted. It consists of power factor correction converter and dc–dc converter for charging the high-voltage battery (HVB) from grid in the grid-to-vehicle (G2V) mode. In particular, its dc–dc converter must precisely regulate the wide ranges of voltage when the HVB is charged. On the other hand, the isolated dc–dc converter is mostly used because the galvanic isolation is required to both reduce the electromagnetic interference noise and satisfy the safety standards. Thus, the associated research has been widely carried out, while improving their overall efficiency and reliability [1], [2], [3], [4], [5], [6], [7], [8], [9], [10], [11], [12], [13], [14], [15], [16], [17], [18], [19]. Recently, the use of EVs as a function of energy storage system are becoming more popular. In this case, the OBC is operated for supplying the energy

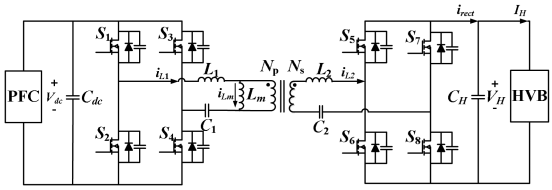

Fig. 1. Circuit configuration of CLLC resonant converter for EVs.

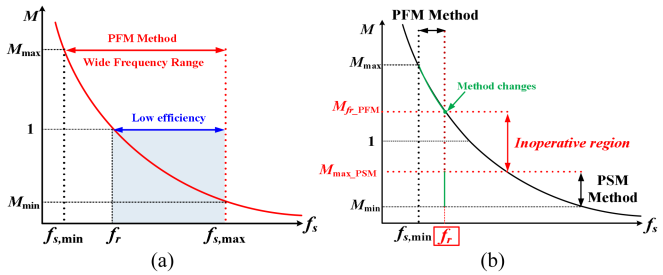

Fig. 2. Conventional control methods for CLLC resonant converter. (a) By conventional PFM control. (b) By conventional PFM-PSM hybrid control in [24], which causes the inoperative region of converter.

of HVB to external loads, such as the grid, home, and other loads. These operations are called as the vehicle-to-grid (V2G), vehicle-to-home, and vehicle-to-load operations, respectively. To meet these requirements, various topologies and control methods for the bidirectional isolated dc–dc converters have been also investigated [11], [12], [13], [14], [15], [16], [17], [18], [19]. Among them, the *CLLC* resonant converter, which is shown in Fig. 1, is being extensively studied because of several advantages in terms of efficiency and power density, which can be obtained due to its wide zero voltage switching (ZVS) operation and high operating frequency.

Conventionally, the *CLLC* resonant converter has been operated by the pulse-frequency modulation (PFM) method, which regulates its V_o by controlling the operating frequency, as shown in Fig. 2(a). However, it has several drawbacks such as the wide ranges of operating frequency, which cause to the first harmonic approximation (FHA) errors, high switching losses, hard commutation, and limited ranges of voltage in the step-down operations, etc. Therefore, for application to the EVs, it uses the variable dc-link voltage control by fixing the operating frequency in order to satisfy load conditions. Nevertheless, this causes high voltage stress when it operates in the wide range. Note that the phase-shift modulation (PSM) method has been widely studied and adopted for various resonant converters to minimize switching loss in their step-down operations [20], [21]. However, it is difficult to perform it in the step-up operation. In other words, there is limitation that can be implemented only for the step-down operation. To handle this, several PFM-PSM hybrid control methods have been studied by combining advantage of each of two methods [22], [23], [24], [25]. For example, the work in [22] simultaneously uses both methods to reduce the switching loss. In particular, it changes the operating frequency to regulate the V_o, while applying the predetermined optimal phase-shift duty ratio to reduce the overall switching

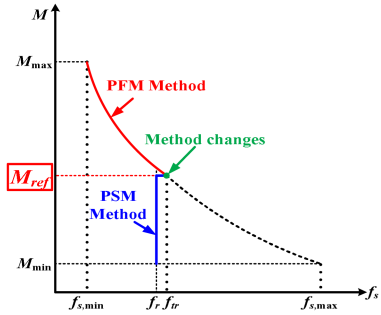

Fig. 3. Featured characteristic of proposed VFSHC method.

loss. However, it still causes high switching loss during the step-down operations because the V_o is regulated by the only PFM method. The other hybrid control methods [23], [24] are applied for the interleaved *LLC* resonant converter. That is, the interleaved PFM method with the PSM compensation is proposed in [23] for reducing the current stress, even under parameter mismatch conditions. Nevertheless, it is difficult to apply this to the single resonant converter topology. This is because it determines the duty ratio of PSM method based on the current imbalance between two resonant converters connected in parallel. In addition, the hybrid control method in [24] changes both methods based on the relationship between f_s [which is determined by the output of proportional-integral (PI) controller] and f_r, as shown in Fig. 2(b). However, it is not feasible to optimally tune the gains of PI-controller in real-time by considering all operating conditions. As the result, it is subject to cause the *inoperative region*, where both methods do not work well, particularly when they suddenly change. Furthermore, this inoperative region can be induced by the relationship between M_{fr_PFM} and $M_{\mathrm{max\_PSM}}$ indicated in Fig. 2(b). It is important to note that it degrades overall efficiency and reliability of converter. Even though the dynamic smooth transition control method adopting the feed-forward voltage is proposed in [25] for reducing the response time and voltage fluctuations when two methods change, it still switches the PFM or PSM method based on the relationship between f_s and $f_{\max}$. Thus, it suffers from the inoperative region like [24].

This article newly proposes the VCR based PFM-PSM hybrid control (VFSHC) method for applying the *CLLC* resonant converter to EVs, while overcoming the limitations of conventional hybrid control methods. The basic concept of proposed VFSHC method is shown in Fig. 3. It changes the PFM and PSM methods based on the relationship between M_{ref}, which can be mathematically determined and M, and then it results in eliminating the inoperative region. In other words, it uses the PSM method when M is lower than M_{ref}. Otherwise, it adopts the PFM method. Therefore, it can improve overall efficiency more effectively than the conventional PFM-PSM hybrid control methods with the inoperative region problem. Also, it can operate the *CLLC* converter in wide ranges of voltages. In particular, the PFM and PSM methods can be seamlessly changed without causing undesired transients by the proposed control method. Furthermore, the new synchronous rectification (SR) method

TABLE I
COMPARISON OF CONTROL METHOD

	Voltage range	Operating frequency range	Single module operation	Reliability	Efficiency
PFM method	Moderate	Wide	O	Moderate	Low
PSM method	Narrow	Narrow	O	High	High
Conventional hybrid control method in [22]	Moderate	Wide	O	Moderate	Moderate
Conventional hybrid control methods in [23], [24]	Wide	Moderate	X	Low	Moderate
Conventional hybrid control method in [25]	Wide	Moderate	O	Low	Moderate
Proposed VFSHC method	**Wide**	**Moderate**	**O**	**High**	**High**

is proposed, and it is adopted to the *CLLC* resonant converter to increase its overall efficiency. Finally, the proposed VFSHC method is compared with several conventional control methods in Table I.

The rest of this article is organized as follows. The characteristic and operational principles of proposed VFSHC method are described in Section II. The design considerations are analyzed in Section III. Then, the practical effectiveness of proposed VFSHC method is verified by experimental tests on the hardware prototype of 1.5 KW in Section IV. Finally, Section V concludes this article.

II. PROPOSED VFSHC METHOD

A. Problems of Conventional Methods

As mentioned above, the conventional PFM methods have several drawbacks like the FHA errors, high switching losses, hard commutation behavior, and limited ranges of V_o in the step-down operations due to its wide ranges of f_s. Also, the conventional hybrid control methods [24], [25] suffer from the inoperative region because they change the PFM and PSM methods based on f_s, which is affected by the gain of PI-controller. In particular, if the gain of PI-controller is low, it is difficult to successfully regulate V_o because f_s is slowly decreased. As the result, the PFM and PSM methods change at $t_{\rm tran}$ where f_s becomes f_r much later than the desired time, t_d, as shown in Fig. 4. In contrast, even when the gain of PI-controller is high, they may still have the inoperative region, where V_o is regulated by continuously changing the PSM and PFM methods, as shown in Fig. 5.

In other words, new switching signals are injected to the CLLC resonant converter based on the relationship between f_r and f_s. This reduces the overall efficiency and reliability of converter. Furthermore, the difference between $M_{fr\_\rm PFM}$ and $M_{\rm max\_PSM}$ can cause the inoperative region, when V_o needs to adjust as the value between $V_{o,\rm max\_PSM}$ and $V_{o,fr\_\rm PFM}$, as shown in Figs. 2(b) and 6.

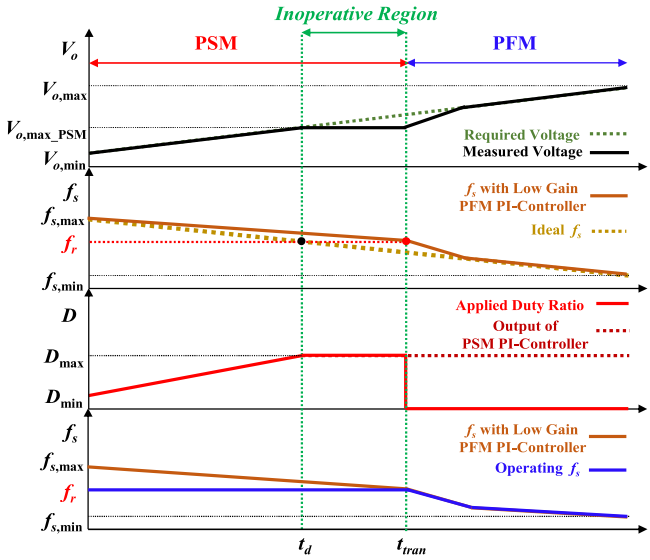

Fig. 4. Operating characteristics of conventional hybrid control methods when the gain of PI-controller is low.

B. Characteristics of Proposed VFSHC Method

The proposed VFSHC method uses the PFM method, when M is higher than $M_{\rm ref}$, which is mathematically computed, as shown in Fig. 3. In contrast, when M becomes lower than $M_{\rm ref}$, the PSM method regulates V_o by controlling D. Note that f_s is fixed to f_r when the PSM method is used. Therefore, it is able to improve the overall reliability of converter, when compared to the conventional PFM method, by reducing the range of f_s, as shown in Fig. 7(a). In addition, it can reduce the switching losses during the step-down operations by fixing f_s corresponding to f_r and eliminating the hard commutation behavior, as shown in Fig. 7(b). Above all, it can solve the inoperative region problem by changing the PFM and PSM methods based on the relationship between $M_{\rm ref}$ and M, which are not affected by the gain of PI-controller. As the result, the proposed VFSHC method can improve the overall efficiency and reliability, particularly when the PFM and PSM methods are changed, as shown in Figs. 8 and 9(b).

When M is higher than $M_{\rm ref}$, the proposed VFSHC method adopts the PFM method to the *CLLC* resonant converter to regulate V_o, similarly to [16]. In this section, the details of how to apply the PSM and SR methods are described when M is lower than $M_{\rm ref}$ as follows.

1) G2V Mode: When the PSM method is applied to the *CLLC* resonant converter, the corresponding operational waveforms are shown in Fig. 10. The phase-shift between the leading and lagging legs of primary H-bridge converter with S_1-S_4 charges the HVB. In addition, the SR control method is also applied to the secondary H-bridge converter with S_5-S_8 to improve the overall efficiency. Each operating mode for the half-cycle is explained in below and the corresponding circuits are shown in Fig. 11.

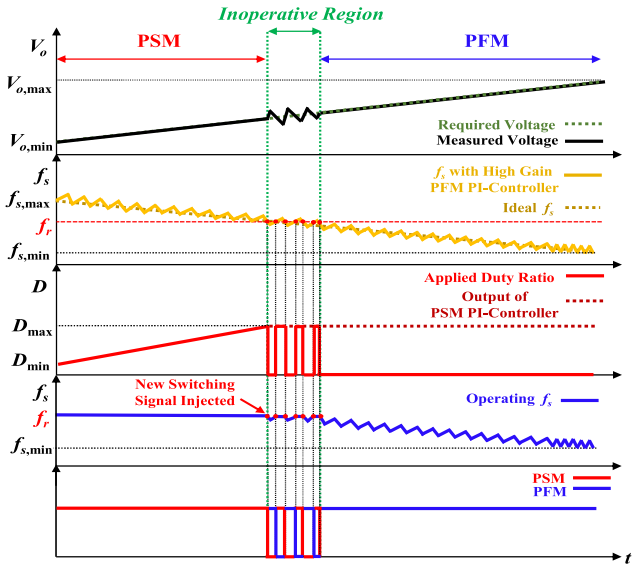

Fig. 5. Operating characteristics of conventional hybrid control methods when the gain of PI-controller is high.

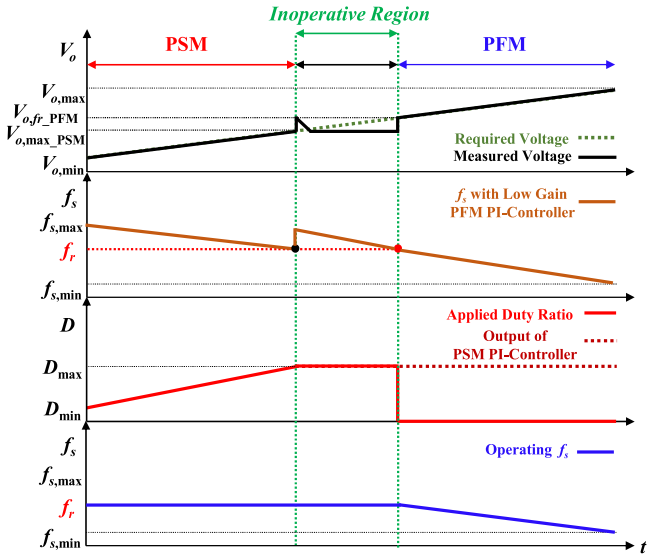

Fig. 6. Operating characteristics of conventional hybrid control methods when $M_{fr,\mathrm{PFM}}$ and $M_{\mathrm{max\_PSM}}$ are different.

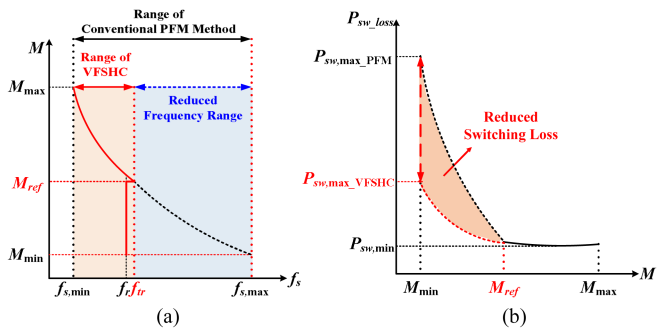

Fig. 7. Characteristics of proposed VFSHC method. (a) Operating frequency range. (b) Switching loss.

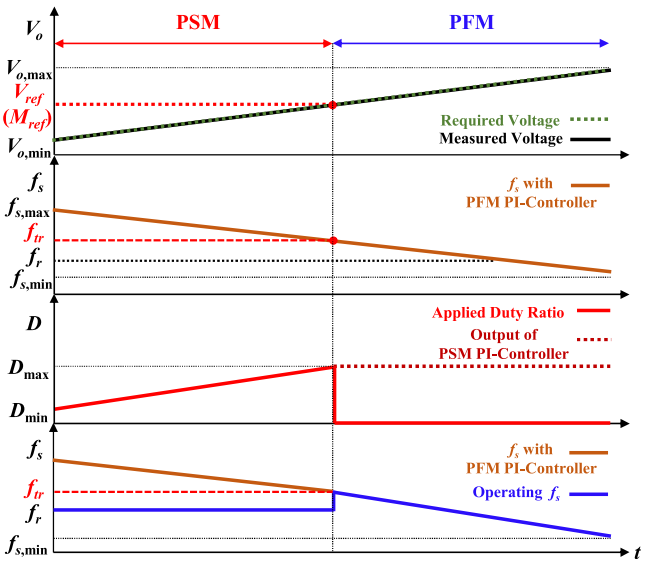

Fig. 8. Operating characteristics of proposed VFSHC method.

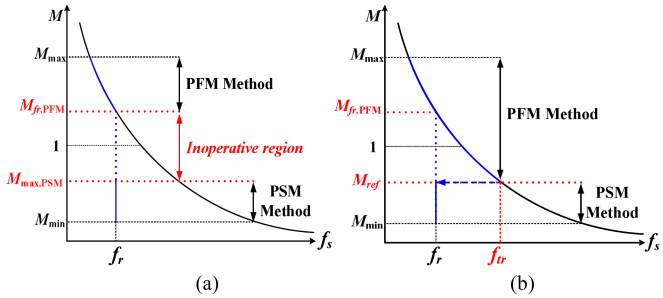

Fig. 9. Comparison of characteristics. (a) By conventional hybrid control method. (b) By proposed VFSHC method.

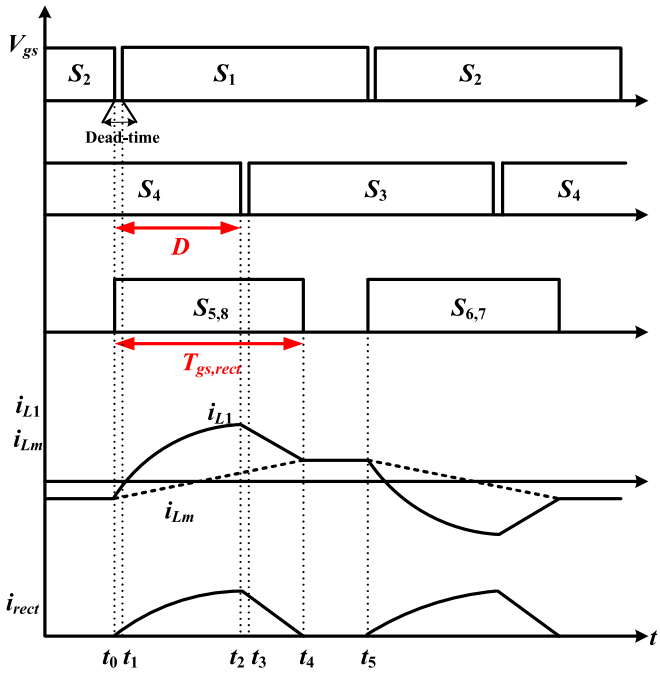

Fig. 10. Operational waveforms of CLLC resonant converter when the PSM method is applied.

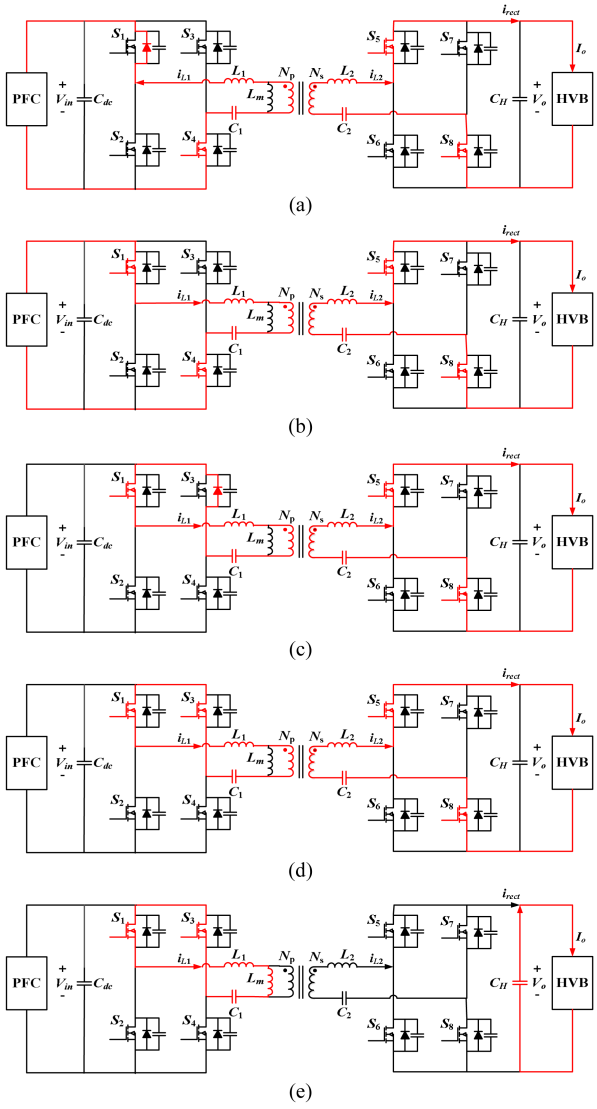

Fig. 11. Operation modes of proposed VFSHC method in G2V mode. (a) Mode 1. (b) Mode 2. (c) Mode 3. (d) Mode 4. (e) Mode 5.

1) *Mode 1* [t_0-t_1]: S_2 is turned OFF at t_0. The primary resonant current, i_{L1} discharges and charges the output capacitances of S_1 and S_2, respectively. Then, i_{L1} flows through the internal diode of S_1 while satisfying the ZVS condition, as shown in Fig. 11(a). Also, the primary resonant inductance, L_1 resonates with the primary resonant capacitance, C_1 to transfer the output power. Then, the magnetizing current, i_{Lm} can be approximated as linearly increasing. Therefore, i_{L1} and i_{Lm} can be represented as

$$i_{L1}(t) = i_{L1}(t_0)\cos(\omega_r(t-t_0)) + \frac{V_{in} - nV_o - V_{c1}(t_0)}{Z_r}\sin(\omega_r(t-t_0))$$

$$i_{Lm}(t) = i_{Lm}(t_0) + \frac{v_{Lm}(t)}{L_m}(t-t_0) \approx i_{Lm}(t_0) + \frac{V_{in}}{L_m}(t-t_0) \quad (1)$$

where ω_r is the resonant frequency, V_{in} is the input voltage, and V_{c1} is the voltage of primary resonant capacitor. In addition, L_m is the magnetizing inductance, n is the turns ratio of transformer, and $Z_r = \sqrt{L_1/C_1}$.

1) *Mode 2* [t_1-t_2]: S_1 is turned ON with the ZVS operation, as shown in Fig. 11(b). In this mode, L_1 resonates with C_1 to transfer the output power, where i_{Lm} can be approximated as linearly increasing, like in mode 1. Therefore, i_{L1} and i_{Lm} can be expressed as

$$i_{L1}(t) = i_{L1}(t_1)\cos(\omega_r(t-t_1)) + \frac{V_{in} - nV_o - V_{c1}(t_1)}{Z_r}\sin(\omega_r(t-t_1))$$

$$i_{Lm}(t) = i_{Lm}(t_1) + \frac{v_{Lm}(t)}{L_m}(t-t_1) \approx i_{Lm}(t_1) + \frac{V_{in}}{L_m}(t-t_1). \quad (2)$$

2) *Mode 3* [t_2-t_3]: S_4 is turned OFF at t_2. The positive i_{L1} charges and discharges the output capacitances of S_4 and S_3. Then, i_{L1} flows through the internal diode of S_3, while satisfying the ZVS condition, as shown in Fig. 11(c). Also, the voltage drops across the primary resonant impedance with L_1 and C_1 and the secondary resonant impedance with L_2 and C_2 are equal to $-(nV_o)/2$ because of symmetric structure of resonant tanks. In addition, the voltage of magnetizing inductance is $(nV_o)/2$. Therefore, it can be approximated that i_{L1} and i_{Lm} decrease and increase linearly, respectively. As the result, i_{L1} and i_{Lm} can be expressed as

$$i_{L1}(t) = i_{L1}(t_2) - \frac{nV_o/2 + V_{c1}(t_2)}{L_1}(t-t_2)$$

$$i_{Lm}(t) = i_{Lm}(t_2) + \frac{nV_o}{2L_m}(t-t_2). \quad (3)$$

3) *Mode 4* [t_3-t_4]: S_3 is turned ON at t_3 with the ZVS operation, as shown in Fig. 11(d). Also, i_{L1} and i_{Lm} have the same characteristics as those in mode 3. Thus, they can be calculated as

$$i_{L1}(t) = i_{L1}(t_3) - \frac{nV_o/2 + V_{c1}(t_3)}{L_1}(t-t_3).$$

$$i_{Lm}(t) = i_{Lm}(t_3) + \frac{nV_o}{2L_m}(t-t_3). \quad (4)$$

4) *Mode 5* [t_4-t_5]: i_{L1} becomes equal to i_{Lm} at t_4. Then, it remains the same as i_{Lm} because the input power is not transferred to the output, as shown in Fig. 11(e). Therefore, i_{L1} and i_{Lm} can be computed as

$$i_{L1}(t) = i_{Lm}(t) = -i_{L1}(t_4). \quad (5)$$

2) V2G Mode: The operational principles in the V2G mode are the same as those in the G2V mode, except that the direction of power flow is reversed. In other words, V_{in} and V_o are determined as the HVB and dc-link voltages, respectively. Then, the phase-shift between the leading and lagging legs of secondary

H-bridge converter regulates the dc-link voltage. Moreover, the SR control method is applied to the primary H-bridge converter.

III. Design Considerations

As well as the proposed SR control method in the G2V mode, several considerations for $M_{\rm ref}$, the ZVS conditions, and loss analysis are mathematically analyzed for the successful operation of proposed VFSHC method.

A. Reference VCR

As mentioned previously, the proposed VFSHC method changes the PFM and PSM methods based on the relationship between M and $M_{\rm ref}$. In particular, $M_{\rm ref}$ is determined by using the voltage conversion ratio (VCR) of *CLLC* resonant converter operated by the PSM method. It can be obtained from the output current and expressed as

$$I_o = \frac{V_o}{R_o} = \frac{2}{T_s}\int_{t_0}^{t_5} i_{L2}(t)dt = \frac{2n}{T_s}\int_{t_0}^{t_4} (i_{L1}(t) - i_{Lm}(t))dt \tag{6}$$

where I_o is the output current, R_o is the load resistance, T_s is the switching period, and i_{L2} is the secondary resonant current. The time periods of t_0-t_2, t_2-t_4, and t_4-t_5 are approximated as

$$t_2 - t_0 = DT_s \tag{7}$$

$$t_4 - t_2 = T_{1-2} \approx \frac{2}{5}\left(\frac{T_s}{2} - DT_s\right)P_k \tag{8}$$

$$t_5 - t_4 = T_{2-3} = \frac{T_s}{2} - (DT_s + T_{1-2}). \tag{9}$$

Note that $P_k{=}P_o\,/P_{o,\rm rated}$, where P_o is the output power and $P_{o,\rm rated}$ is the rated output power. Then, i_{L1} at t_0 and the voltages across C_1 at t_2 and t_0 can be represented as

$$i_{L1}(t_0) = -\frac{1}{2L_m}\left(V_{\rm in}DT_s + \frac{nV_o}{2}T_{1-2}\right). \tag{10}$$

$$\begin{aligned} V_{C1}(t_2) &= V_{C1}(t_0) + \frac{1}{C_1}\int_{t_0}^{t_2} i_{L1}(t)dt \\ &= V_{C1}(t_0)\left(1 - \frac{1-\cos(\omega_r DT_s)}{Z_r C_1 \omega_r}\right) \\ &\quad + \frac{1}{C_1\omega_r} i_{L1}(t_0)\sin(\omega_r DT_s) \\ &\quad + \frac{V_{\rm in} - nV_o}{Z_r C_1 \omega_r}(1-\cos(\omega_r DT_s)). \end{aligned} \tag{11}$$

$$\begin{aligned} V_{C1}(t_0) = &\\ &\frac{V_{\rm in}\left(k - \frac{T^2{}_{1-2}}{2L_2}\right) - nV_o\left(k - \frac{T^2{}_{1-2}}{4L_1}\right) + i_{L1}(t_0)\left(\frac{\sin(\omega_r DT_s)}{\omega_r}\right)}{k - 2C_1} \\ &+ \frac{T_{1-2}\cos(\omega_r DT_s) - \frac{T^2{}_{1-2}}{2L_1 C_1 \omega_r}\sin(\omega_r DT_s) - \left(\frac{T_s}{2} - (T_{1-2}+D)\right)}{k - 2C_1} \end{aligned} \tag{12}$$

where k is determined as

$$\begin{aligned} k = &\frac{1-\cos(\omega_r DT_s)}{Z_r\omega_r} + \frac{T_{1-2}}{Z_r}\sin(\omega_r DT_s) \\ &+ \frac{T^2{}_{1-2}}{2L_1}\left(1 - \frac{1-\cos(\omega_r DT_s)}{Z_r C_1 \omega_r}\right) \end{aligned} \tag{13}$$

Finally, the VCR of *CLLC* resonant converter operated by the PSM method is determined by (14) which is shown at the bottom of the next page, where B_1 and B_2 are described in (15), which is shown at the bottom of the next page. Thereafter, $M_{\rm ref}$ is selected by the maximum VCR in (14) for this article with the safety margin to effectively utilize the advantages of PSM method during the step-down operation.

B. Zero-Voltage Switching Condition

The ZVS operation must be achieved to improve overall efficiency and reliability. Then, several factors in below are considered.

1) ZVS Energy: The inductive energy must be larger than the capacitive energy to charge and discharge the output capacitances of switches, which are participating in the ZVS operation. Then, the following condition must be satisfied regardless of which method is applied to the CLLC resonant converter [27]

$$t_{\rm dead} \geq 16 C_{\rm oss} f_s L_m \tag{16}$$

where $t_{\rm dead}$ is the dead time, and $C_{\rm oss}$ is the output capacitance of switch. In this regard, the ZVS energy condition of *CLLC* resonant converter operated by the PSM method can be given as

$$|i_{Lm}(t_0)| = \frac{1}{2}\left(\frac{V_{\rm in}}{L_m}D + \frac{nV_o}{2L_m}T_{1-2}\right) \geq I_c = 2C_{\rm oss}\frac{V_{\rm in}}{t_{\rm dead}} \tag{17}$$

$$t_{\rm dead} \geq \frac{4C_{\rm oss}V_{\rm in}}{\frac{V_{\rm in}}{L_m}D + \frac{nV_o}{2L_m}T_{1-2}} \tag{18}$$

where I_c is the current required to charge and discharge the output capacitances.

2) Direction of Current: The direction of current must be carefully considered such that it flows through the internal diode of switch before it is turned on to achieve the ZVS operation, as shown in Fig. 11(a). As the result, the following conditions must be satisfied.

$$i_{L1}(t_o) < 0 \text{ and } i_{L1}(t_2) > 0. \tag{19}$$

C. Loss Analysis

The power losses of *CLLC* resonant converter are mainly composed of conduction loss, switching loss, core loss of transformer, and winding loss of transformer. However, the winding loss of transformer is negligible because it is much lower than other power losses. Therefore, the conduction loss, switching loss, and core loss of transformer is analyzed for this article.

1) Conduction Loss: The conduction loss of *CLLC* resonant converter can be calculated as [28]

$$P_{\rm cond} = 2(I^2{}_{L1,\rm rms}R_{\rm ds,on} + I^2{}_{L2,\rm rms}R_{\rm ds,on}) \tag{20}$$

where P_{cond} is the conduction loss, $I_{L1,\text{rms}}$ is the rms value of i_{L1}, $I_{L2,\text{rms}}$ is the rms value of i_{L2}, and $R_{\text{ds,on}}$ is the drain-source on-resistance of switches. Also, i_{L1} and i_{L2} (rms values) by the PSM and PFM methods are obtained as

$$I_{L1,\text{rms\_PSM}} = \frac{2}{T_s}\sqrt{\int_{t_o}^{t_0+\frac{T_s}{2}} {i_{L1}}^2(t)dt} \tag{21}$$

$$I_{L1,\text{rms\_PFM}} = \frac{{V_o}^2}{8}\left[\left(\frac{T_s}{2L_m}\right)^2 + \left(\frac{\pi}{R_o}\right)^2\right] \tag{22}$$

$$I_{L2,\text{rms\_PSM}} = \frac{2n}{T_s}\sqrt{\int_{t_o}^{t_0+\frac{T_s}{2}} \left(i_{L1}(t) - i_{Lm}(t)\right)^2 dt} \tag{23}$$

$$I_{L2,\text{rms\_}PFM} = \frac{{V_o}^2}{16}\left[\frac{(5\pi^2-48)T_s}{12\pi^2 L_m} + \frac{1}{{R_o}^2}\right]. \tag{24}$$

2) Switching Loss: The turn-on loss is assumed to be negligible when the ZVS operations of all switches are achieved. Then, the turn-OFF loss of *CLLC* resonant converter operated by the PSM method is computed as

$$P_{\text{off1,2}} = \frac{1}{3}\left(|i_{L1}(t_0)| - C_{\text{oss}}\frac{V_{\text{in}}}{t_{\text{fall}}}\right)V_{\text{in}}t_{\text{fall}}f_s \tag{25}$$

$$P_{\text{off3,4}} = \frac{1}{3}\left(|i_{L1}(t_2)| - C_{\text{oss}}\frac{V_{\text{in}}}{t_{\text{fall}}}\right)V_{\text{in}}t_{\text{fall}}f_s \tag{26}$$

$$P_{\text{off5-8}} = \frac{2}{3}\left(|i_{L2}(t_4)| - C_{\text{oss}}\frac{V_o}{t_{\text{fall}}}\right)V_o t_{\text{fall}}f_s \tag{27}$$

where $P_{\text{off1,2}}$, $P_{\text{off3,4}}$, and $P_{\text{off5-8}}$ are the turn-OFF losses of (S_1 and S_2), (S_3 and S_4), and (S_5−S_8), respectively. Also, t_{fall} is the fall time of switches. Then, the total turn-OFF loss can be determined as

$$P_{\text{off}} = P_{\text{off\_priamry}} + P_{\text{off\_secondary}} = P_{\text{off 1,2}} + P_{\text{off 3,4}} + P_{\text{off 5-8}} \tag{28}$$

where $P_{\text{off primary}}$ and $P_{\text{off secondary}}$ are the turn-OFF loss of primary and secondary H-bridge converters, respectively. In particular, when the PFM method is used, $P_{\text{off primary}}$ is approximately equal to the twice of $P_{\text{off 34}}$ by (26), and $P_{\text{off secondary}}$ is almost same as $P_{\text{off 5-8}}$ by (27).

3) Core Loss of Transformer: The peak-to-peak magnetic flux density, ΔB_T and rate of change of magnetic flux density, dB_T/dt must be determined in order to analyze the total core loss [28], [29]. Firstly, ΔB_T is computed as

$$\Delta B_T = \frac{V_{\text{in}}D + \frac{nV_o}{2}T_{1-2}}{N_p A_e} \tag{29}$$

where N_p is the number of turns of primary winding, and A_e is the effective cross-sectional area of transformer. Next, dB_T/dt is calculated as

$$\frac{dB_T(t)}{dt} = \begin{cases} \frac{V_{\text{in}}}{N_p A_e}, t \in [t_o, t_2] \\ \frac{nV_o}{2N_p A_e}, t \in [t_2, t_4] \end{cases}. \tag{30}$$

As the result, the core loss of transformer can be obtained as

$$P_{\text{core}} = \frac{2}{T_s}V_T\int_{t_0}^{t_0+\frac{T_s}{2}} k_i\left|\frac{dB_T(t)}{dt}\right|^{\alpha}(\Delta B_T)^{\beta-\alpha}dt \tag{31}$$

where P_{core} is the core loss of transformer, and V_T is the volume of magnetic core. Also, α and β are the magnetic characteristic coefficients of core, and k_i is expressed as

$$k_i = \frac{k_{co}}{(2\pi)^{\alpha-1}\int_0^{2\pi}|\cos\theta|\,2^{\beta-\alpha}d\theta} \tag{32}$$

where k_{co} is the magnetic characteristic coefficient. Finally, the total efficiency can be expressed as

$$\eta = \frac{P_o}{P_o + P_{\text{loss,total}}} = \frac{P_o}{P_o + P_{\text{cond}} + P_{\text{off}} + P_{\text{core}}} \tag{33}$$

where η and $P_{\text{loss,total}}$ are the efficiency and total loss of *CLLC* resonant converter, respectively.

D. Synchronous Rectification Control Method

The conventional SR control methods [30], [31], [32], [33] suffer from several drawbacks such as requirements of auxiliary circuits, voltage and current sensors, and high complexity of control. To overcome these limitations, the time period of gate signal for the switches in the rectifying H-bridge converter, $T_{gs,\text{rect}}$ is calculated by using (7) and (8), and it is used for allowing the rectifier current to flow only through the channel of switches instead of internal diode. In the G2V mode, $T_{gs,\text{rect}}$ is determined and applied to the switches in the secondary H-bridge converter, as shown in Fig. 10. It can be calculated as

$$T_{gs,\text{rect}} = t_4 - t_0 = \left(\left(1 - \frac{2}{5}P_k\right)D + \frac{1}{5}P_k\right)T_s. \tag{34}$$

$$\text{VCR} = \frac{nV_o}{V_{\text{in}}} = \frac{\left(\frac{D}{4L_mL_1C_1\omega_r}\sin(\omega_r DT_s) - \frac{1}{2L_1}\right){T^2}_{1-2} - \frac{D}{2L_m}\left(1+\cos(\omega_r DT_s)\right)T_{1-2} - \frac{D}{2L_m\omega_r}\sin(\omega_r DT_s) + k - \frac{B_1}{k-2C_1}k}{\frac{T_s}{2n^2R_o} - \frac{\sin(\omega_r DT_s)}{8L_mL_1C_1\omega_r}{T^3}_{1-2} + \frac{1}{4}\left(\frac{\cos(\omega_r DT_s)}{L_m} - \frac{1}{L_1}\right){T^2}_{1-2} + \frac{1}{4L_m}\left(\frac{\sin(\omega_r DT_s)}{\omega_r} - D\right)T_{1-2} + k - \frac{k}{k-2C_1}B_2} \tag{14}$$

$$B_1 = k - \frac{{T^2}_{1-2}}{2L_1} - \frac{D}{2L_m\omega_r}\sin(\omega_r DT_s) - \frac{D}{2L_m}T_{1-2}\cos(\omega_r DT_s) + \frac{{T^2}_{1-2}D}{4L_mL_1C_1\omega_r}\sin(\omega_r DT_s) + \frac{D}{4L_m}T_s - \frac{D}{2L_m}T_{1-2} - \frac{D^2}{2L_m}$$

$$B_2 = k - \frac{{T^2}_{1-2}}{4L_1} + \frac{T_{1-2}}{4L_m\omega_r}\sin(\omega_r DT_s) + \frac{{T^2}_{1-2}}{4L_m}\cos(\omega_r DT_s) - \frac{{T^3}_{1-2}}{8L_mL_1C_1\omega_r}\sin(\omega_r DT_s) - \frac{T_{1-2}}{8L_m}T_s + \frac{{T^2}_{1-2}}{4L_m} + \frac{T_{1-2}}{4L_m}D. \tag{15}$$

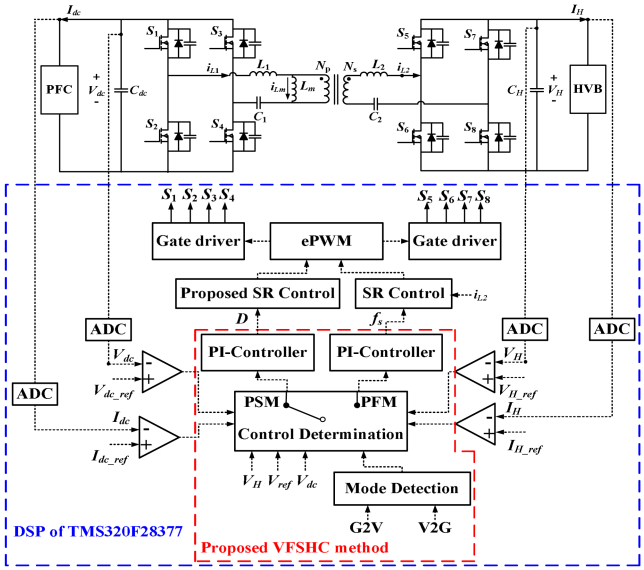

Fig. 12. Control diagram of proposed VFSHC method.

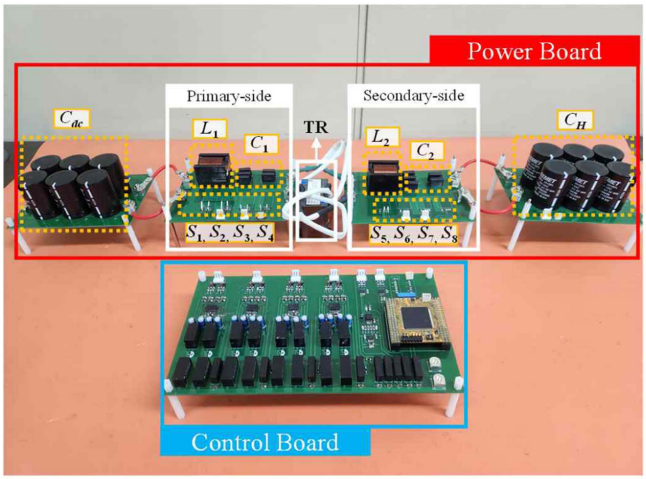

Fig. 13. Hardware prototype of *CLLC* resonant converter.

IV. Experimental Verifications

The control diagram to implement the proposed VFSHC method is shown in Fig. 12. Firstly, the operating mode is selected. Then, it determines which of PFM and PSM methods is applied to the *CLLC* resonant converter. Thereafter, the SR control method is properly employed according to the applied PFM or PSM method to improve the overall efficiency.

Then, the experimental tests are conducted on the hardware prototype of 1.5 KW to verify the practical effectiveness of proposed VFSHC method, as shown in Figs. 13 and 14. The values of parameters are given in Table II. The voltage and power ratings of hardware prototype are downscaled when compared to those of commercial system. This is because there are limitations of experimental laboratory environment. In other words, the voltage range of HVB is determined as 200−350 V, and the dc-link voltage is set to 300 V. Then, the digital signal processor of TMS320F28377 is adopted to implement the proposed VFSHC method. The dc power supply of SGI600/25 is used for providing the input voltage within the range required by the HVB.

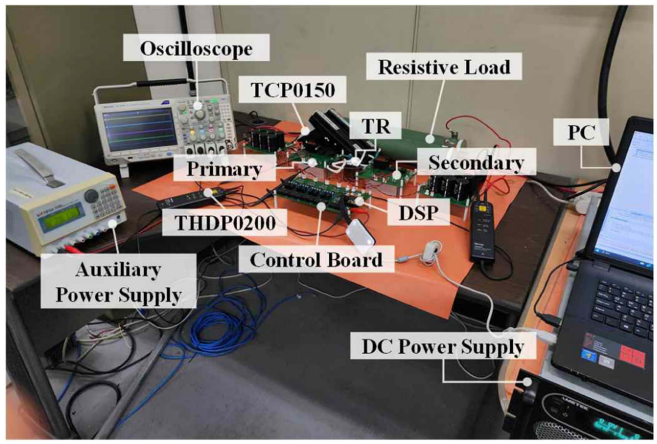

Fig. 14. Hardware setup for the experimental test.

TABLE II
Parameters of Proposed *CLLC* Resonant Converter

Parameters	Values
Power rating	1.5 KW
DC-link voltage (V_{dc})	300 V
Voltage of HVB (V_H)	200–350 V
DC-link capacitor (C_{dc})	450 μF
HVB capacitor (C_H)	450 μF
Turns ratio of transformer (N_p: N_s)	1:1
Resonant inductances (L_1, L_2)	23 μH
Resonant capacitances (C_1, C_2)	100 nF
Magnetizing inductance (L_m)	110 μH
Resonant frequency (f_r)	104.94 kHz
Reference VCR (M_{ref})	0.95
Reference voltage (V_{ref})	285 V
SiC MOSFETs (S_1–S_8)	NTH4L040N120SC1 (1200 V/58 A)

Also, the oscilloscopes of MDO 3054 and MSO58 5-BW-500, differential voltage probe of THDP0200, and current probe of TCP0150 are used to measure the voltage, current, and efficiency.

In particular, the silicon carbide (SiC) MOSFETs of NTH4L040N120SC1 are utilized to establish S_1-S_8 of *CLLC* resonant converter. The transformer is implemented using PQ50/50 ferrite cores, and its volume is determined as 128.03 cm^3. Also, the turns ratio of transformer (N_p:N_s) is set to 1:1, and M_{ref} is determined to be 0.95 considering (14) and the safety margin.

Then, the proposed VFSHC method changes the PFM and PSM methods when V_{ref} is equal to V_H in the G2V mode. In other words, it uses the PFM and PSM methods in the G2V mode when $V_H > V_{\text{ref}}$ and $V_H \leq V_{\text{ref}}$, respectively. Note that the experimental tests in the only G2V mode are carried out because the operational characteristics in the V2G mode are the same as those in the G2V mode.

When the PSM method is used, the experimental results are shown in Figs. 15 and 16. It is observed that the PSM method

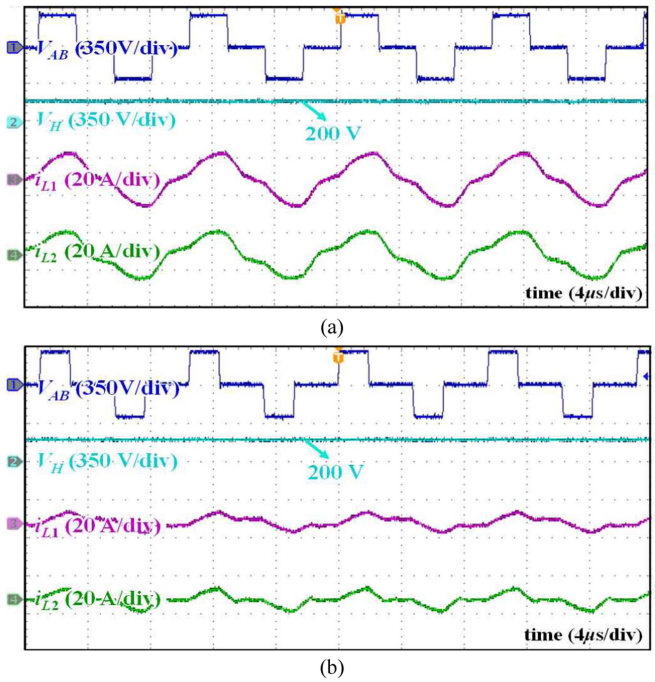

Fig. 15. Experimental results of proposed VFSHC method when $V_H = 200$ V. (a) Waveforms at full load. (b) Waveforms at 30% load.

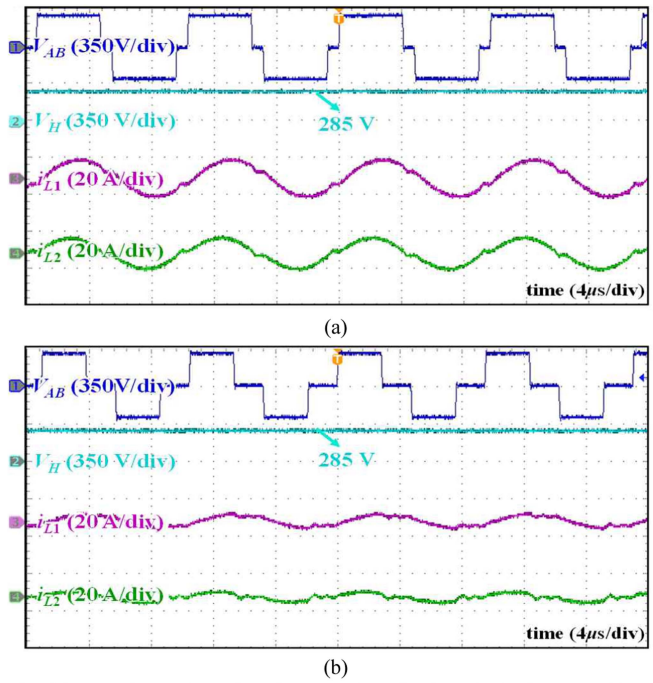

Fig. 16. Experimental results of proposed VFSHC method when $V_H = 285$ V. (a) Waveforms at full load. (b) Waveforms at 30% load.

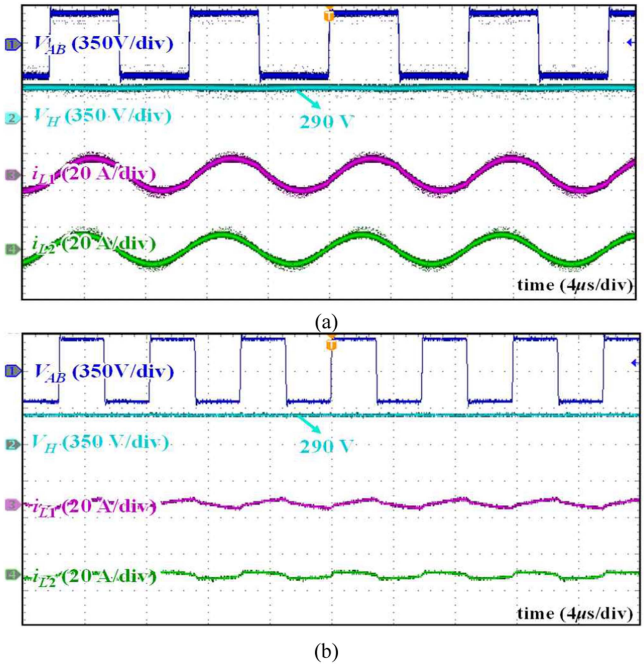

Fig. 17. Experimental results of proposed VFSHC method when $V_H = 290$ V. (a) Waveforms at full load. (b) Waveforms at 30% load.

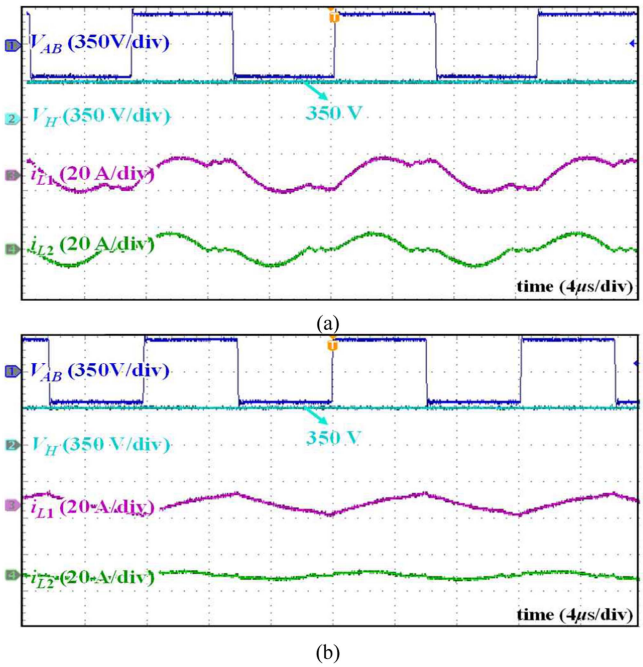

Fig. 18. Experimental results of proposed VFSHC method when $V_H = 350$ V. (a) Waveforms at full load. (b) Waveforms at 30% load.

successfully regulates the voltage in the range of $V_H \leq V_{\text{ref}}$. In other words, the proposed VFSHC method can regulate the voltage range of HVB from 200 to 285 V under both 30% and full load conditions. In contrast, note that the proposed VFSHC method applies the PFM method to the *CLLC* resonant converter when V_H keep increasing, and therefore V_H becomes greater than V_{ref}. These experimental results are shown in Figs. 17 and 18. It is observed that the PFM method can effectively regulate the voltage range of $V_H > V_{\text{ref}}$. In other words, the proposed VFSHC method can regulate the voltage range of HVB from 285 to 350 V under both 100% and 30% load conditions. Also, the experimental results by the proposed SR control method are shown in Figs. 19and 20. They clearly prove

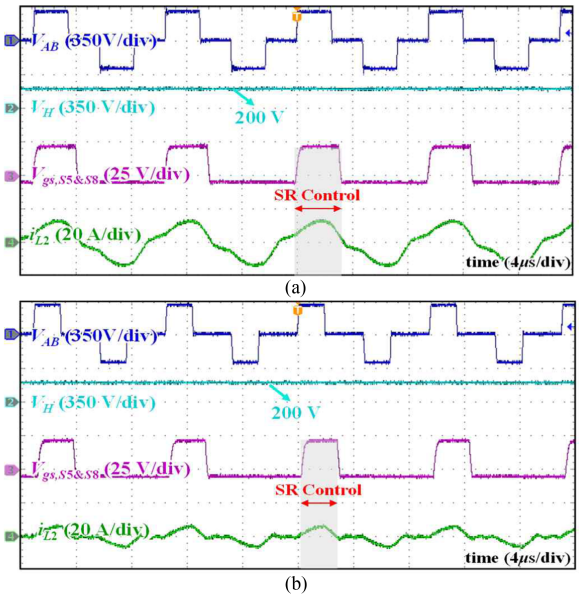

Fig. 19. Experimental results of proposed SR control method when V_H = 200 V. (a) Waveforms at full load. (b) Waveforms at 30% load.

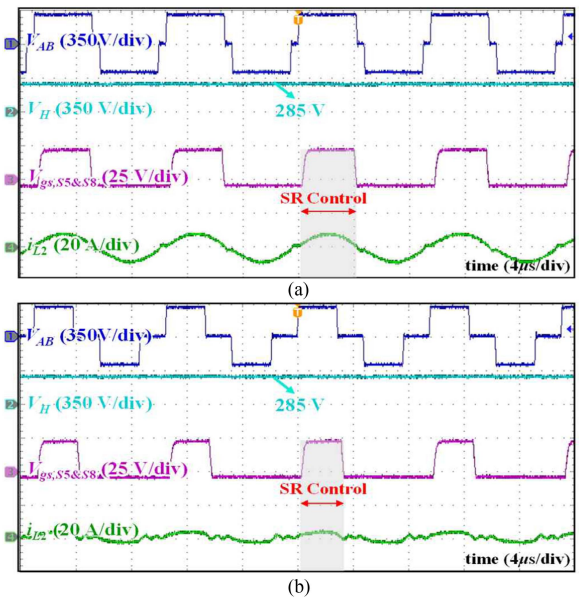

Fig. 20. Experimental results of proposed SR control method when V_H = 285 V. (a) Waveforms at full load. (b) Waveforms at 30% load.

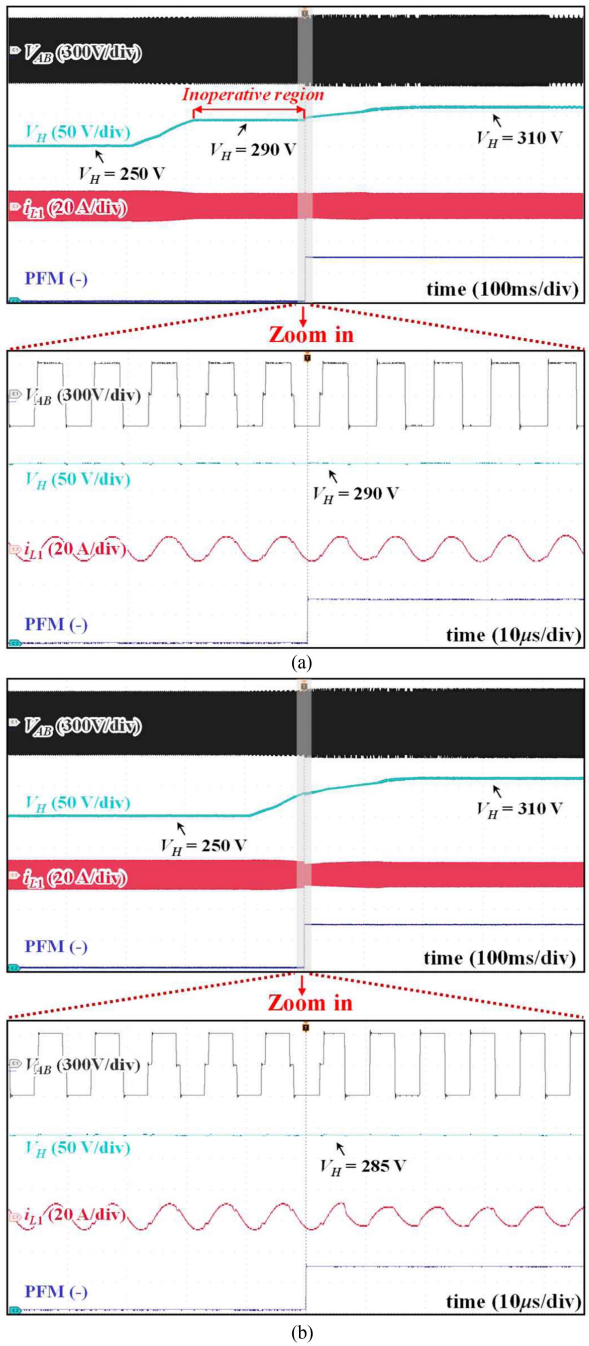

Fig. 21. Comparison of dynamic performance. (a) Conventional hybrid control method when the gain of PI-controller is low. (b) Proposed VFSHC method when the gain of PI-controller is low.

that the proposed SR control method can successfully make the secondary current to flow through the channels of switches rather than the internal diodes, when the proposed VFSHC method applies the PSM method. In particular, it is observed that the proposed SR control method is successfully applied at the full load condition, as shown in Figs. 19(a) and 20(a). Furthermore, it performs effectively under the load condition of 30%, as shown in Figs. 19(b) and 20(b).

Moreover, to compare the dynamic performances by both the conventional hybrid control and proposed VFSHC methods, the additional experimental tests are conducted when the voltage of HVB is increased from 250 to 310 V. The results are shown in Figs. 21 and 22. When the PFM signal (which is indicated by the blue line) is high, the proposed VFSHC method applies the PFM method. Otherwise, the *CLLC* resonant converter is operated by the PSM method. Then, when the gain of PI-controller is low, it is observed from Fig. 21(a) that the conventional hybrid control method exhibits the inoperative region, as shown in Fig. 4. In other words, the voltage of HVB is maintained at the maximum voltage by the PSM method (290 V) until f_s becomes lower than f_r. On the contrary, when the same low-gain of PI-controller is

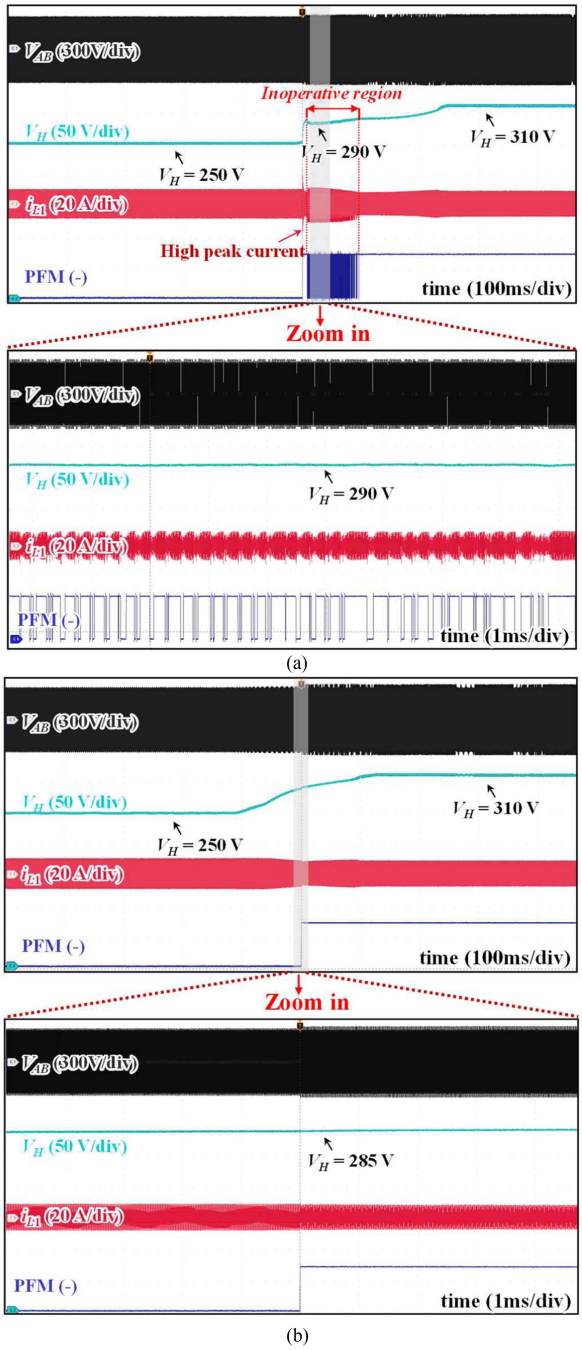

Fig. 22. Comparison of dynamic performance. (a) Conventional hybrid control method when the gain of PI-controller is high. (b) Proposed VFSHC method when the gain of PI-controller is high.

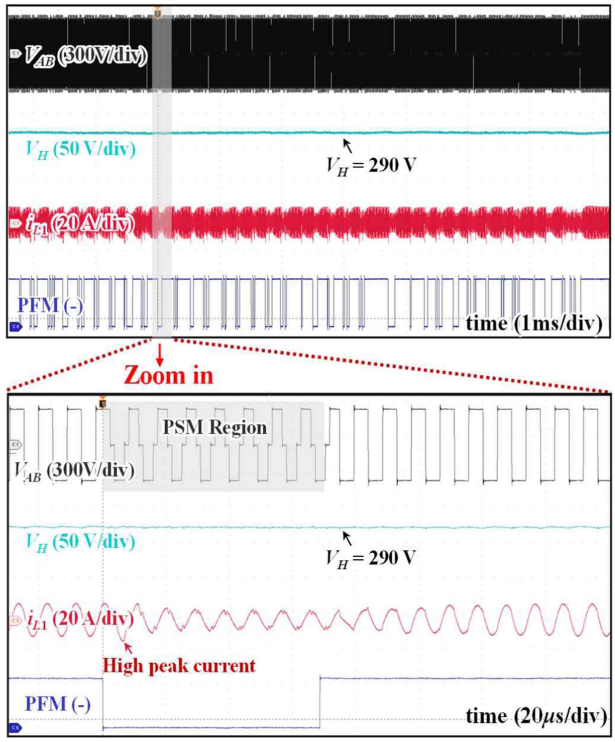

Fig. 23. Dynamic waveforms of conventional hybrid control method when the gain of PI-controller is high.

used for the proposed VFSHC method, the entire range of V_o is successfully regulated, as shown in Fig. 21(b). Furthermore, even when the gain of PI-controller is high, the conventional hybrid control method still suffers from the inoperative region, as shown in Fig. 22(a). This is because the new switching signals are injected whenever f_s becomes same as f_r when the conventional hybrid control method is used. Therefore, the high current stress is induced to the *CLLC* resonant converter, and it can reduce the overall reliability, as shown in Fig. 22(a). However, the proposed VFSHC method can smoothly change the PFM and PSM methods and successfully regulate V_o without experiencing the inoperative region, when the same gain of PI-controller is used, as shown in Fig. 22(b). Note that these experimental results in Figs. 21 and 22 have the very good agreement with the theoretical analysis in Figs. 4 and 5 for defining the inoperative region caused by the conventional hybrid control method.

Then, they clearly prove that it decreases the overall reliability of converter. In particular, the proposed VFSHC method can decrease the current stress by 24% compared to the conventional hybrid control method, as shown in Figs. 23 and 24. In other words, the proposed VFSHC method has superior dynamic performance compared to the conventional hybrid control method, regardless of the gain of PI-controller.

Finally, the efficiencies of proposed VFSHC method when $V_H \leq V_{\text{ref}}$ are measured and compared with those of conventional PFM method at various HVB voltages and load conditions.

The results are shown in Fig. 25. It is observed that the proposed VFSHC method achieves the maximum efficiency of 95.12% under the HVB voltage of 285 V and load condition of 80%

Furthermore, the proposed VFSHC method improves the overall efficiency compared to the conventional PFM method. In particular, the proposed VFSHC method improves the efficiency by 4.59% when the HVB voltage is 200 V.

In summary, the proposed VFSHC method can successfully regulate the wide ranges of voltage while eliminating the inoperative region by changing the PFM and PSM methods based

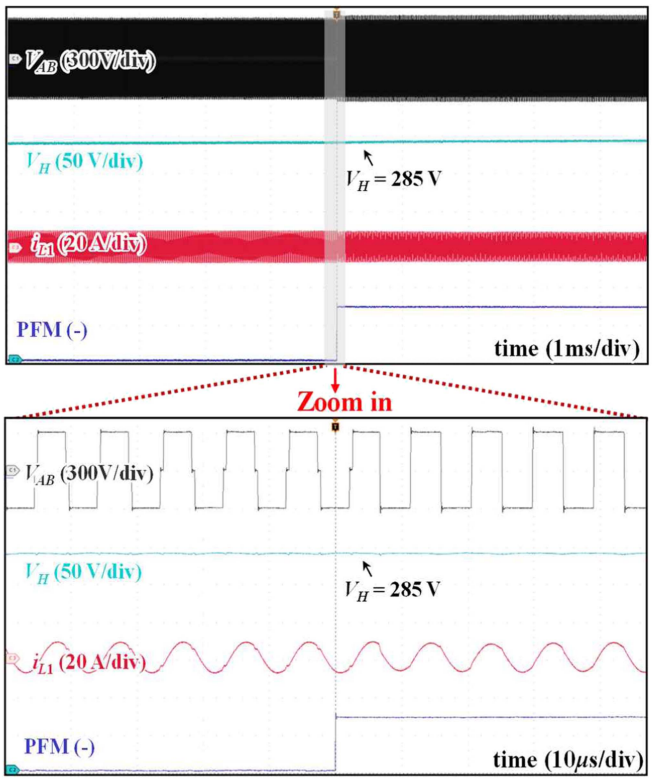

Fig. 24. Dynamic waveforms of proposed VFSHC method when the gain of PI-controller is high.

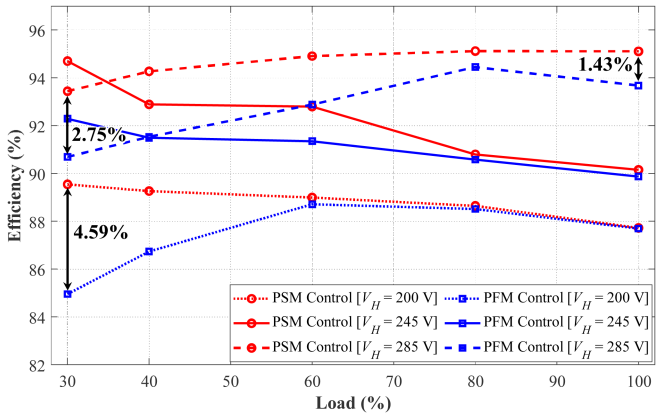

Fig. 25. Comparison of efficiency.

on M_{ref}. Furthermore, it can improve the overall efficiency and reliability compared to the conventional PFM and PFM-PSM hybrid control methods.

V. Conclusion

This article newly proposes the VFSHC method of *CLLC* resonant converters for EVs. The proposed VFSHC method can successfully regulate the wide ranges of voltage by changing the PFM and PSM methods based on the relationship between M_{ref} and M, which are not affected by the gain of PI-controller. In addition, it can enhance the overall efficiency compared to the conventional PFM method by applying the PSM method when M is lower than M_{ref}. Furthermore, the proposed VFSHC method can increase the overall reliability when compared to the conventional PFM-PSM hybrid control methods by removing the inoperative region and reducing the current stress. In summary, the proposed VFSHC method has several advantages over the conventional PFM and PFM-PSM hybrid control methods as follows.

1) Wide ranges of voltage.
2) High efficiency.
3) High reliability.
4) Seamless control in mode changes.

The practical effectiveness of proposed VFSHC method is fully verified through the experimental tests conducted on the hardware prototype of 1.5 KW. The proposed VFSHC method successfully regulates the wide ranges of voltage while eliminating the inoperative region. In addition, it improves the overall reliability, particularly when the PFM and PSM methods are changed, by reducing the current stress by 24% when compared to the conventional PFM-PSM hybrid control methods. Furthermore, it improves efficiency by 4.59% over the conventional PFM method under the HVB voltage of 200 V and load condition of 30%.

References

[1] I. O. Lee and G. W. Moon, "Half-bridge integrated ZVS full-bridge converter with reduced conduction loss for electric vehicle battery chargers," *IEEE Trans. Ind. Electron.*, vol. 60, no. 8, pp. 3978–3988, Aug. 2014.

[2] K. Jong-Soo, C. Gyu-Yeong, J. Hye-Man, and L. Byoung-kuk, "Design and implementation of a high-frequency on-board battery charger for electric vehicles with frequency control strategy," in *Proc. IEEE Veh. Power Propulsion Conf.*, Sep. 2010, pp. 1–6.

[3] M. Yilmaz and P. T. Krein, "Review of battery charger topologies, charging power levels, and infrastructure for plug-in electric and hybrid vehicles," *IEEE Trans. Power Electron.*, vol. 28, no. 5, pp. 2151–2169, May 2013.

[4] N. Tan, T. Abe, and H. Akagi, "Design and performance of a bidirectional isolated DC–DC converter for a battery energy storage system," *IEEE Trans. Power Electron.*, vol. 27, no. 3, pp. 1237–1248, Mar. 2012.

[5] M. Pahlevaninezhad, P. Das, J. Drobnik, P. K. Jain, and A. Bakhshai, "A novel ZVZCS full-bridge DC/DC converter used for electric vehicles," *IEEE Trans. Power Electron.*, vol. 27, no. 6, pp. 2752–2769, Jun. 2012.

[6] H. Wang, S. Dusmez, and A. Khaligh, "Maximum efficiency point tracking technique for LLC-based PEV chargers through variable dc link control," *IEEE Trans. Ind. Electron.*, vol. 61, no. 11, pp. 6041–6049, Nov. 2014.

[7] T. Kim, S. Lee, and W. Choi, "Design and control of the phase shift full bridge converter for the on-board battery charger of the electric forklift," in *Proc. 8th Int. Conf. Power Electron.—ECCE Asia*, 2011, pp. 2709–2716.

[8] D. Moon, J. Park, and S. Choi, "New interleaved current-fed resonant converter with significantly reduced high current side output filter for EV and HEV applications," *IEEE Trans. Power Electron.*, vol. 30, no. 8, pp. 4264–4271, 2015.

[9] R. Hou, P. Magne, B. Bilgin, and A. Emadi, "A topological evaluation of isolated DC/DC converters for Auxiliary power modules in electrified vehicle applications," in *Proc. IEEE Appl. Power Electron. Conf. Expo.*, Mar. 2015, pp. 1360–1366.

[10] W. J. Lee, C. E. Kim, G. W. Moon, and S. K. Han, "A new phase-shift full-bridge converter with voltage-doubler-type rectifier for high-efficiency PDP sustaining power module," *IEEE Trans. Ind. Electron.*, vol. 55, no. 6, pp. 2450–2458, Jun. 2008.

[11] A. Taylor, G. Liu, H. Bai, A. Brown, P. Johnson, and M. McAmmond, "Multiple-phase-shift control for a dual active bridge to secure zero-voltage switching and enhance light-load performance," *IEEE Trans. Power Electron.*, vol. 33, no. 6, pp. 4584–4588, Jun. 2018.

[12] P. He and A. Khaligh, "Comprehensive analyses and comparison of 1 kW isolated DC–DC converters for bidirectional EV charging systems," *IEEE Trans. Transp. Electrific.*, vol. 3, no. 1, pp. 147–156, Mar. 2017.
[13] B. Zhao, Q. Song, and W. Liu, "Efficiency characterization and optimization of isolated bidirectional DC–DC converter based on dual-phase-shift control for DC distribution application," *IEEE Trans. Power Electron.*, vol. 28, no. 4, pp. 1711–1727, Apr. 2013.
[14] X. Liu et al., "Novel dual-phase-shift control with bidirectional inner phase shifts for a dual-active-bridge converter having low surge current and stable power control," *IEEE Trans. Power Electron.*, vol. 32, no. 5, pp. 4095–4106, May 2017.
[15] S. Bal, D. B. Yelaverthi, A. K. Rathore, and D. Srinivasan, "Improved modulation strategy using dual phase shift modulation for active commutated Current-Fed dual active bridge," *IEEE Trans. Power Electron.*, vol. 33, no. 9, pp. 7359–7375, Sep. 2018.
[16] J.-H. Jung, H.-S. Kim, M.-H. Ryu, and J.-W. Baek, "Design methodology of bidirectional CLLC resonant converter for high-frequency isolation of DC distribution systems," *IEEE Trans. Power Electron.*, vol. 28, no. 4, pp. 1741–1755, Apr. 2013.
[17] W. Chen, P. Rong, and Z. Lu, "Snubberless bidirectional DC–DC converter with new CLLC resonant tank featuring minimized switching loss," *IEEE Trans. Ind. Electron.*, vol. 57, no. 9, pp. 3075–3086, Sep. 2010.
[18] S. Zou, J. Lu, A. Mallik, and A. Khaligh, "Bi-directional CLLC converter with synchronous rectification for plug-In electric vehicles," *IEEE Trans. Ind. Appl.*, vol. 54, no. 2, pp. 998–1005, Mar./Apr. 2018.
[19] Z. U. Zahid, Z. M. Dalala, R. Chen, B. Chen, and J.-S. Lai, "Design of bidirectional DC–DC resonant converter for vehicle-to-grid (V2G) applications," *IEEE Trans. Transp. Electrific.*, vol. 1, no. 3, pp. 232–244, Oct. 2015.
[20] U. Mumtahina and P. J. Wolfs, "Multimode optimization of the Phase-Shifted LLC series resonant converter," *IEEE Trans. Power Electron.*, vol. 33, no. 12, pp. 10478–10489, Dec. 2018.
[21] B. Xue, H. Wang, J. Liang, Q. Cao, and Z. Li, "Phase-shift modulated interleaved LLC converter with ultrawide output voltage range," *IEEE Trans. Power Electron.*, vol. 36, no. 1, pp. 493–503, Jan. 2021.
[22] J.-H. Kim, C.-E. Kim, J.-K. Kim, J.-B. Lee, and G.-W. Moon, "Analysis on load-adaptive phase-shift control for high efficiency full-bridge LLC resonant converter under light-load conditions," *IEEE Trans. Power Electron.*, vol. 31, no. 7, pp. 4942–4955, Jul. 2016.
[23] K. Murata and F. Kurokawa, "An interleaved PFM LLC resonant converter with phase-shift compensation," *IEEE Trans. Power Electron.*, vol. 31, no. 3, pp. 2264–2272, Mar. 2016.
[24] H. Wu, X. Zhan, and Y. Xing, "Interleaved LLC resonant converter with hybrid rectifier and variable-frequency plus phase-shift control for wide output voltage range applications," *IEEE Trans. Power Electron.*, vol. 32, no. 6, pp. 4246–4257, Jun. 2017.
[25] C.-Y. Tang, C.-W. Wang, and H.-C. Chien, "A dynamic smooth transition control integrated with hybrid modulation for wide output voltage range bidirectional CLLC resonant converters," *IEEE Trans. Power Electron.*, vol. 38, no. 11, pp. 13587–13593, Nov. 2023.
[26] I. Kim, W.-Y. Jang, M.-W. Kim, and J.-W. Park, "PFM-PSM hybrid controlled CLLC resonant converter for electric vehicles," in *Proc. Energy Convers. Congr. Expo*. Oct. 2023, pp. 3386–3391.
[27] X. Li, J. Huang, Y. Ma, X. Wang, J. Yang, and X. Wu, "Unified modeling, analysis, and design of isolated bidirectional CLLC resonant DC–DC converters," *IEEE J. Emerg. Sel. Top. Power Electron.*, vol. 10, no. 2, pp. 2305–2318, Apr. 2022.
[28] T. Zhu, F. Zhuo, F. Zhao, F. Wang, H. Yi, and T. Zhao, "Optimization of extended phase-shift control for full-bridge CLLC resonant converter with improved light-load efficiency," *IEEE Trans. Power Electron.*, vol. 35, no. 10, pp. 11129–11142, Oct. 2020.
[29] I. Villar, U. Viscarret, I. Etxeberria-Otadui, and A. Rufer, "Global loss evaluation methods for nonsinusoidally fed medium-frequency power transformers," *IEEE Trans. Ind. Electron.*, vol. 56, no. 10, pp. 4132–4140, Oct. 2009.
[30] X. Xie, J. C. P. Liu, F. N. K. Poon, and M. H. Pong, "A novel high frequency current-driven synchronous rectifier applicable to most switching topologies," *IEEE Trans. Power Electron.*, vol. 16, no. 5, pp. 635–648, Sep. 2001.
[31] H. Pan, Y. C. Liang, and R. Oruganti, "Design of smart power synchronous rectifier," *IEEE Trans. Power Electron.*, vol. 14, no. 2, pp. 308–315, Mar. 1999.
[32] C. Sun, Q. Sun, R. Wang, P. Zhang, L. Zhang, and P. Wang, "Universal synchronous rectification scheme for LLC resonant converter using primary-side inductor voltage," *IEEE Trans. Ind. Electron.*, vol. 70, no. 6, pp. 5747–5759, Jun. 2023.
[33] X. Zhu et al., "A sensorless model-based digital driving scheme for synchronous rectification in 1-kV input 1-MHz GaN LLC converters," *IEEE Trans. Power Electron.*, vol. 36, no. 7, pp. 8359–8369, Jul. 2021.

Issac Kim (Member, IEEE) received the B.S. and Ph.D. degrees in power electronics from the School of Electrical and Electronic Engineering, Yonsei University, Seoul, Korea, in 2019 and 2024, respectively.

He is currently a Postdoctoral Research Associate with the School of Electrical and Electronic Engineering, Yonsei University. His research interests include dc–dc converter, on-board charger and dc fast charger for electric vehicles, integrated power converter, and hardware implementation of power converters.

Won-Yong Jang (Student Member, IEEE) received the B.S. degree in power electronics from the Department of Electrical Engineering, Soong-sil University, Seoul, Korea, in 2022. He is currently working toward the Ph.D. degree in power electronics via the combined M.S. and Ph.D. program from Yonsei University, Seoul, Korea.

His research interests include dc–dc converter, resonant dc–dc converter, on-board charger and dc fast charger for electric vehicles, and hardware implementation of power converters.

Seung-Jun Lee (Student Member, IEEE) received the B.S. degree in power electronics in 2024 from the School of Electrical and Electronic Engineering, Yonsei University, Seoul, South Korea, where he is currently working toward the Ph.D. degree in power electronics via the combined M.S. and Ph.D. program.

His research interests include dc–dc converter, on-board charger and dc fast charger for electric vehicles, and integrated power converter.

Jung-Wook Park (Senior Member, IEEE) was born in Seoul, Korea. He received the B.S. degree (summa cum laude) in power system and power electronics from the Department of Electrical Engineering, Yonsei University, Seoul, Korea, in 1999, and the M.S.E.C.E. and Ph.D. degrees from the School of Electrical and Computer Engineering, Georgia Institute of Technology, Atlanta, USA, in 2000 and 2003, respectively.

He was a Post-doctoral Research Associate with the Department of Electrical and Computer Engineering, University of Wisconsin, Madison, WI, USA, during 2003–2004, and a Senior Research Engineer with LG Electronics Inc., South Korea, during 2004–2005. Since 2005, he has been with the School of Electrical and Electronic Engineering, Yonsei University, Seoul, Korea, where he is currently a Professor. His current research interests include power system dynamics, energy management system, renewable energies based distributed generation system, operation and planning of microgrid, and hardware implementation of power-electronic based inverters, etc

Dr. Park was the recipient of Young Scientist Presidential Award in 2013 from the Korean Academy of Science and Technology, Korea. He is also the Director of Yonsei-power system research center of great energy transition (Yonsei-PREFER) supported by the leading research program (with the $7.2M USD grant for nine years from 2020 to 2029) of National Research Foundation, South Korea.